Physically Derived Sound Synthesis Model of a Propeller

Rod Selfridge[*]
Queen Mary University of London
London, UK
r.selfridge@qmul.ac.uk

David Moffat[†]
Queen Mary University of London
London, UK
d.j.moffat@qmul.ac.uk

Joshua D Reiss[‡]
Queen Mary University of London
London, UK
joshua.reiss@qmul.ac.uk

ABSTRACT

A real-time sound synthesis model for propeller sounds is presented. Equations obtained from fluid dynamics and aerodynamics research are utilised to produce authentic propeller-powered aircraft sounds. The result is a physical model in which the geometries of the objects involved are used in sound synthesis calculations. The model operates in real-time making it ideal for integration within a game or virtual reality environment. Comparison with real propeller-powered aircraft sounds indicates that some aspects of real recordings are not replicated by our model. Listening tests suggest that our model performs as well as another synthesis method but is not as plausible as a real recording.

CCS CONCEPTS

• **Human-centered computing** → **User models**; • **Applied computing** → **Sound and music computing**; *Physics*; *Media arts*;

KEYWORDS

Physical Model, Sound Synthesis, Real-Time.

ACM Reference Format:
Rod Selfridge, David Moffat, and Joshua D Reiss. 2017. Physically Derived Sound Synthesis Model of a Propeller. In *Proceedings of AM '17, London, United Kingdom, August 23–26, 2017,* 8 pages.
https://doi.org/10.1145/3123514.3123524

[*]Rod Selfridge is a PhD candidate within EECS Dept., QMUL. Supported by EPSRC, grant EP/G03723X/1
[†]David Moffat is a PhD candidate within EECS Dept., QMUL.
[‡]Joshua Reiss is a Professor within, EECS Dept., QMUL.

AM '17, August 23–26, 2017, London, United Kingdom

ACM ISBN 978-1-4503-5373-1/17/08…$15.00
https://doi.org/10.1145/3123514.3123524

Figure 1: Example of a four bladed propeller driven aircraft - North American P51 Mustang

1 INTRODUCTION

The development of real-time sound synthesis models has great potential for use in nonlinear media such as video games and virtual reality. A sound synthesis model that reacts in real-time to the variety of perspectives and interactions within these environments can offer an increased sense of realism that replaying of sampled sounds fails capture. Linear media such as film and television also benefit from the bespoke sound effects our model is capable of producing.

The motivation for such a model is to produce a sound effect based on the physics of the propeller from the perspective of an observer at any position in the virtual environment. We present the context of a propeller driven aeroplane, such as the one shown in Fig. 1, where the major noise contributing source is the propeller used for propulsion. This is a proof of concept design and it is envisaged that the model can be extended to more aircraft, including helicopters.

The propeller model is part of a series of sound effects that fall under a category of sounds known as *aeroacoustics*. An aeroacoustic sound is generated when air flows around or over an object. As the air flows around the object, oscillating forces and pressure changes can occur, perceived as sound by a listener.

For a 100 years or more, vehicle design has improved and the speeds reached by aircraft, cars, trains, etc. has greatly increased. Research into aeroacoustic noise has found it is one of the main sources of discomfort for passengers, a potential

cause for structural damage [1] and limits the operation of some high speed trains [2].

Semi-empirical equations are ones where an assumption or generalisation has been made to simplify the calculation or yield results in accordance with observations. They are used by aeroacoustic engineers to diminish complex computations yet provide accurate acoustic results. Relevant equations from this field have been identified based on tangible parameters, allowing us to build a physical model sound effect.

2 STATE OF THE ART

One of the main techniques for solving fluid dynamic problems and calculating aeroacoustic noise is to use Computational Fluid Dynamics (CFD) software. Software packages are complicated, requiring the fluid domain to be modelled using a mesh. The fundamental fluid dynamics equations (Navier-Stokes equations) can then be solved using techniques like the finite volume method. These calculations can take from hours to weeks to obtain a solution, depending on techniques employed and level of detail required.

Physical modelling synthesis was presented in [3] where a number of models are presented, including a clarinet and a Helmholtz resonator. These are implemented using delay lines and filters based on the physical geometry of the objects.

The use of High Performance Computing (HPC) platforms can accelerate the computational processes to obtain real time operation. In [4] a Field Programmable Gate Array (FPGA) was employed to solve finite difference equations representing the physical model of an 5 string banjo.

Real-time examples of fan and rotor sound synthesis were presented in [5] where an appreciation of the physics behind the sound generating process has informed each model. The fan sounds are generated by varying the speed of pulses as the speed of the blades varies. A similar frequency is calculated in our implementation but used as the centre frequency of a bandpass filter. We also calculate harmonics, propagation characteristics and vortex sounds.

A physically derived model of a compact sound source representing the Aeolian tone was presented in [6]. This is then extended in [7], where a number of sources are used to replicate the sound of a sword, bat or club. The same compact sound source was used in a portion of our propeller model, described in Section 4. A real-time physical model of an aeroacoustic musical instrument was presented in [8] using similar techniques along with mechanical properties of a string.

A different approach was taken in [9] where sounds are synthesised to represent the interior of aircraft for designers to evaluate noise pollution. An analysis of recorded sounds are evaluated in the Fourier domain and then re-synthesised in real time. Jet aeroplane noise is synthesised in [10]. This identifies that some of the tonal sounds are generated by wheel well cavities when the landing gear is extended. An analysis approach is used to identify tonal components in aircraft noise which are then synthesised by use of a sine wave with time-varying amplitude and frequency. Perceptual tests revealed that tonal noise above 4000 Hz was annoying. Therefore prediction of this, along with simultaneous broadband aircraft noise, are useful for designers.

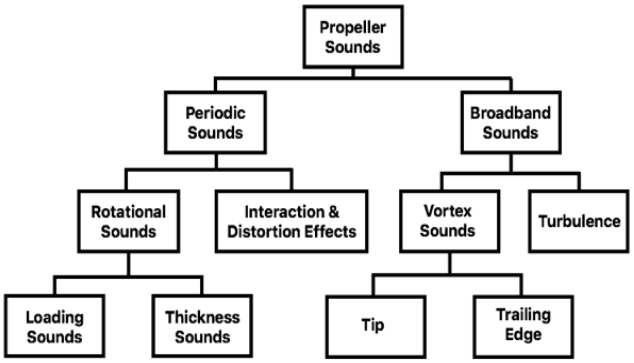

Figure 2: Different sources of aeroacoustic noise associated with propellers, rotors and lift fans. Adapted from [12].

An extension of the Kirchhoff integral to produce a multipole expansion (monopole, dipole and quadrupole) of the aeroacoustic sound of a propeller was given in [11]. The purpose of an analytical derivation of the sound produced in the far field is to allow propeller designers to apply reverse engineering. By setting the far field noise to acceptable levels at specific observer positions, selective propeller parameters can be ascertained.

Our requirements for a propeller sound effect is to produce a model that captures many of the characteristics of the aeroacoustic sounds based on the physics of the interactions while operating in real-time. The model should have relevant parameters allowing real-time interaction by a sound designer or game engine. Much of this research exploits techniques and semi-empirical equations developed by aircraft engineers before the computational power required to solve the fundamental equations was available.

3 METHOD

A comprehensive review of the sound generated by propellers, rotors and lift fans is given by [12]. Fig. 2 shows a breakdown of the different sound generating processes. The sources under the heading of Interaction and Distortion Effects are not considered in our propeller model as these are associated with helicopter rotors. The local coordinate used to calculate sound radiation patterns is shown in Figs 3.

A main sources of aeroacoustic sound is from *loading sounds*. Sounds are generated by air pressure surrounding a

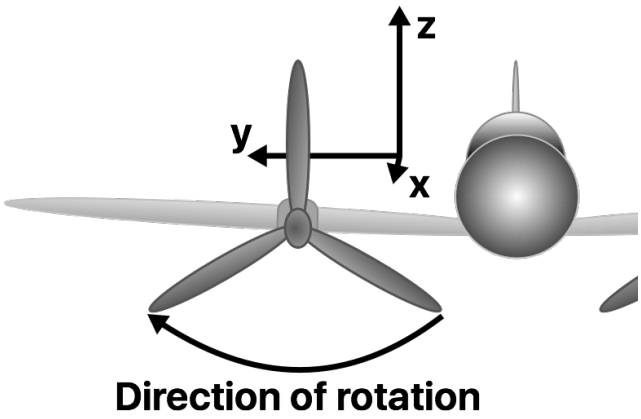

Figure 3: Local coordinates of spinning propeller

propeller blade as air passes over it. There is a thrust component which is a pressure force normal to the plane of rotation of the propeller and a torque component which is a pressure component within the propeller plane. Under uniform conditions the two forces will be steady with respect to the blade. When viewed from a stationary reference point in the disc of a rotating propeller, the pressure will pulsate as the blade passes this point. This generates a harmonic sound source at the blade passing frequency. The separate and combined sound radiation patterns for thrust and torque are shown in Figs. 4a, 4b and 4d.

Thickness noise is the sound generated as the blade moves the air aside when passing. This sound is found to be small when blades are moving at the speed of sound, 343 m/s, (known as a speed of Mach 1), and is not considered in our model [12].

The dominant broadband sources are *vortex sounds* which are created as each blade cuts through the air. A significant body of research has been carried out in relation to vortices being shed as objects move through the air and the sounds generated are known as Aeolian tones. The vortices are generated at a given frequency as the propeller blade cuts though the air and depends on the speed of air over the object. The radiation pattern for the vortex sounds is shown in Fig 4c. An equation giving the frequency of vortex shedding f_{st} is given in Eqn. 1.

$$f_{st} = \frac{S_t u}{d} \tag{1}$$

where u is the airspeed, d the diameter and a value known as the Strouhal number S_t. Since the speed u is highest at the tip and slower towards the centre a wide band of sound is generated. The mean acoustic intensity, $\overline{I_l(t)}$, of the sound generated is proportional to u^6 as given in Eqn. 2, (simplified from [13]).

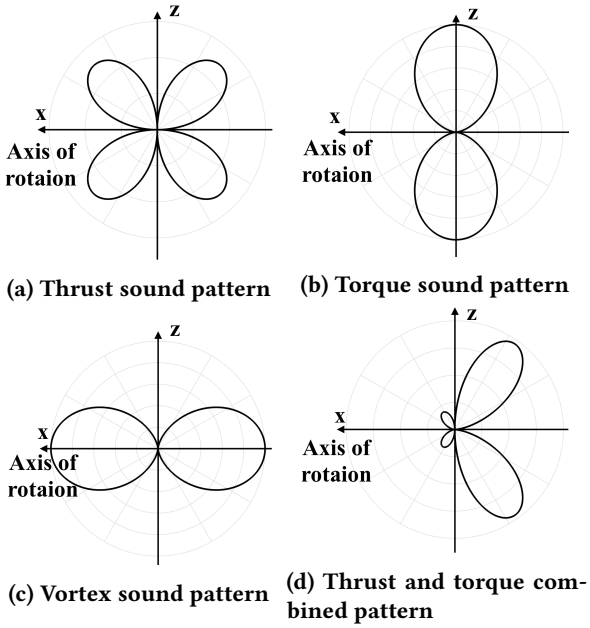

Figure 4: Sound radiation patterns based on local coordinates

$$\overline{I_l(t)} \sim \frac{\sqrt{2\pi} S_t^2 \rho\, u^6 sin^2\theta cos^2\varphi}{32c^3 r^2 (1 - Mcos\theta)^4} \tag{2}$$

where ρ is the density of air, θ and φ the elevation and azimuth, c the speed of sound, r the distance between source and observer, and M is the Mach number, $M = u/c$.

The turbulence sounds are pseudorandom noises from vortices generated by interactions with air and the propeller. This noise is usually from inefficient sources and classed as insignificant compared to other sources although can be significant if interacting with the pressure field of a moving propeller blade. This noise is not replicated in our model.

Therefore the two main sources of propeller sounds that will be replicated by our model are loading sounds and vortex sounds.

4 IMPLEMENTATION

The graphical programming language *Pure Data* was used to implement the propeller model. This was chosen since the code is open source and ease of reproducibility was preferred over high performance computations.

Aircraft Models

A number of aircraft and their propellers were replicated to demonstrate the scope and properties of our model. A central reason for choice of aircraft is access to recorded samples of the same aircraft allowing as close a comparison as possible

Table 1: Aircraft models and relevant data. ‡ - Best estimate based on visual examination of blade images. ⊕ - modified noting blade chord length almost a constiant 0.47m [14]. ⋆ - profile taken from RAF drawing

Model	Top Speed (m/s)	RPM	Engine Power (HP)	Blade Radius (m)	Blade Profile ‡
Hercules C13[1]	164	1020	4590	2.06	NACA 16 ⊕
Boeing B17[2]	144	2500	1200	1.63	RAF[3] ⋆
Tiger Moth[4]	48	2100[5]	130	0.99[6]	RAF ⋆
Yakovlev Yak-52[7]	79	1860[8]	360	1.20[9]	NACA 16
Cessna 340[10]	125	2500[11]	310	0.96	ARA-D
P51 Mustang[12]	193	1280[13]	1490	1.70	NACA 16

between real recordings and synthesis models, (Section 5). Table 1 shows the aircraft models and data obtained.

Loading Sounds

Appendix B in [12] provides a 'Generalized Propeller-Noise Estimating Procedure'. Ten steps predict the sound pressure level of the fundamental loading sounds including harmonics. Many of the steps require reading values from graphs which have been approximated by the authors, enabling the model to authentically adjust parameters in real time; equations are provided and readers are referred to [12] for the original graphs. Steps where a graph has been approximated are highlighted with an asterisk (*); remaining steps are calculated from given equations. All sound pressure level (SPL) values, L_x, are given in dBs.

(1) Obtain a reference sound pressure level L_α relating power input to the propeller:

$$L_\alpha[n] = 15.11 \log(P[n]) + 83.57 \tag{3}$$

where $P[n]$ is the engine power, units of horse power.

(2) Correct for the number of blades and blade diameter:

$$L_\beta = 20 \log \frac{4}{B} + 40 \log \frac{4.72}{D} \tag{4}$$

where B is the number of blades and D is the propeller diameter.

(3) Obtain correction factor accounting for the speed of propeller rotation and distance between propeller and *point of interest*, (stated as 1 foot ≈ 0.305m, [12]):

$$L_\gamma[n] = (25.12 M_T[n] - 33.40) \log \frac{0.305}{D} + (34.37 M_T[n] - 36.88) \tag{5}$$

where $M_T[n]$ is the Mach number of the blade tip.

(4) Obtain the directional correction factor, taking into account the directional characteristics of a propeller. This is similar to Gutin's theory of propeller acoustics illustrated in [13], where the greatest acoustic intensity is given at approximately 120° to the direction of flight:

$$L_\delta[n] = -5.3\text{x}10^{-3}\theta^2[n] + 1.19\theta[n] - 62.32 \tag{6}$$

where $\theta[n]$ is the azimuth angle between source and observer. A minimum value of −20dB is set to match measured plots given in [15].

(5) Correct for spherical attenuation of sound relative to distance between observer and source:

$$L_\epsilon[n] = -20 \log(3.375 r[n] - 1) \tag{7}$$

where $r[n]$ is the distance between observer and source in metres.

(6) Sum all the SPL values to obtain value at the reference point.

$$L_\zeta[n] = L_\alpha[n] + L_\beta + L_\gamma[n] + L_\delta[n] + L_\epsilon[n] \tag{8}$$

(7) Calculate the harmonic distribution of sound up to the 10th harmonic:

$$H_N[n] = 26 e^{-(-0.7 M_T[n] + 0.79)N} - 22 \tag{9}$$

where $H_N[n]$ is the gain of each harmonic (dB) and N is the harmonic number.

(8) The values obtained for $H_N[n]$, with $N \in [1, 10]$ are subtracted from $L_\zeta[n]$ to give individual SPL values for each harmonic.

(9) Approximate values for atmospheric absorption for each harmonic $A_N[n]$ are calculated from Table 2. The attenuation values are subtracted for each harmonic.

$$L_\zeta[n] - H_N[n] - A_N[n] \tag{10}$$

[1] en.wikipedia.org/wiki/Lockheed_C-130_Hercules
[2] alternatewars.com/SAC/B-17G_Flying_Fortress_SAC_-_27_April_1949.pdf
[3] i178.photobucket.com/albums/w252/YavorD/PropellorRAFT5291BE2C2D.jpg
[4] en.wikipedia.org/wiki/De_Havilland_Tiger_Moth
[5] rafjever.org/tigpic027
[6] hercprops.com/in-stock/
[7] en.wikipedia.org/wiki/Yakovlev_Yak-52
[8] airbum.com/pireps/PirepYak-52.html
[9] 76.222.206.206/yak52/specs
[10] en.wikipedia.org/wiki/Cessna_340
[11] aopa.org/go-fly/aircraft-and-ownership/aircraft-fact-sheets/cessna-340
[12] en.wikipedia.org/wiki/North_American_P-51_Mustang
[13] spitfireperformance.com/mustang/mustangtest

Table 2: Approximate values for atmospheric absorption for each frequency band, † estimate by authors

Frequency Bands (Hz)	Attenuation from noise source, $A_N[n]$ (dB per 1000 feet)
[0, 90)	0
[90, 180)	0.2
[180, 355)	0.6
[355, 710)	1
[710, 1400)	1.8
[1400, 2800)	3.3
[2800, 5600)	6
[5600, 11,200)	11.4
> 11,200	20†

(10) These are then converted back to linear gain values G_N.

$$G_N[n] = 2\text{x}10^{-5} \,.\, 10^{\frac{L_{\tilde{\zeta}}[n]-H_N[n]-A_N[n]}{20}} \tag{11}$$

The frequency for each harmonic of the loading sound, f_{L_N} is calculated in Eqn. 12.

$$f_{L_N}[n] = \frac{NB \,.\, \text{RPM}[n]}{60} \tag{12}$$

where RPM[n] stands for revolutions per minute. Each harmonic is implemented as noise filtered by a variable bandpass filter where the passband of the filter is centred on the harmonic frequency. The harmonic gain value was set to the value calculated in step 10.

Vortex Sounds

Compact sound source models from [6] are used to synthesise vortex sound. To replicate a propeller blade a number of these sources are 'placed' in a row to represent different points on a propeller blade, similar to [7]. Each blade is represented by 7 compact sources.

The main difference found in relation to a propeller blade compared with the cylinder modelled presented in [6] is that the fundamental frequency of Eqn. 1 was found to correspond to a Strouhal number $St = 0.85$ [16] as opposed to $St \approx 0.2$ for a cylinder. The diameter used in Eqn. 1 to calculate the frequency becomes the propeller *chord length* and each harmonic frequency f_{st_N} is shown in Eqn. 13:

$$f_{st_N}[n] = \frac{0.85Nu[n]}{\text{Chord Length}} \tag{13}$$

The different chord lengths and chord positions along the length of the blade were all obtained from a historical RAF blade profile[3]. We calculate the speed of each source $u[n]$ using the source radius and RPM[n] value. Two other propeller blade profiles were presented in [17]. These are labelled *NACA 16* and *ARA-D* and similar data were obtained from these two profiles and applied to the synthesis model.

The gain is calculated from a discrete implementation of Eqn. 2.

Motor Sounds

The propeller in an aeroplane is not heard in isolation; the motor is often a major sound source. How loudly we hear the motor depends on its characteristics, distance and any masking by aeroacoustic sounds. Missing the roughness associated with a four stroke propeller motor may have perceptual implications. The fuel supply mixture may also be relevant. Depending on era these may be normally aspirated, fuel injected or turbo. It was not the purpose of our design to replicate the motor component so a model was adapted from the helicopter sound effect in [5]. A very small random factor was added to the RPM value for each propeller unit to model small differences between the engines.

5 RESULTS

Exact comparisons between recorded samples and our physical models are limited. When examining the output signal of the recordings, details of the operating conditions and flight paths were not provided. Therefore aircraft speed, distance and propeller RPM were unknown. Recordings only provided details of the type of aircraft; propeller dimensions and other properties have been obtained to try and give as fair an evaluation as possible.

Objective Evaluation

A comparison between a recorded sample and a sample from our physical model was performed. The recorded sample was of a Cessna, taken from the BBC Sound Effect Library, (AircraftCessna.BBC.EC1A4b.wav). The Cessna is a small light propeller powered aircraft but further model details such as the model number are unknown.

Our physical model was made to replicate a Cessna 340. This aircraft has two propellers, each with three blades. Our model travels at a speed of 100 m/s, engine of 300 horse power, propellers spinning at 2200 RPM and a blade length of 0.96m. The physical model moves in virtual space from south east to north west of the observer, on a heading of 319°. A sine-cosine law is used for panning. The distance varies from 370m at the closest point to 1163m when furthest away and descends from a height of 325m to 50m at a pitch of 7.9° down. Time, spectrogram and magnitude plots are shown in Fig. 5 for both the recorded sample and physical model.

The time plots of Figs. 5a and 5b show a similar increase of amplitude as the aircraft passes the observer. Both recordings have the aircraft moving from right lower red plot to left upper blue plot across the stereo field. This is indicated

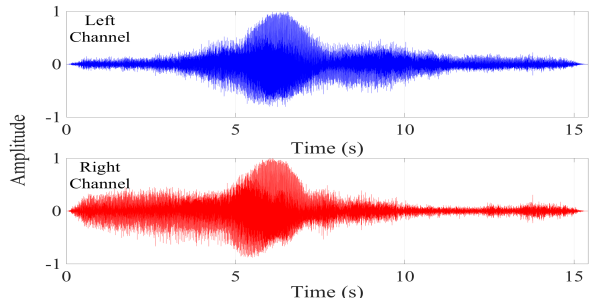

(a) Time plot of recorded propeller plane.

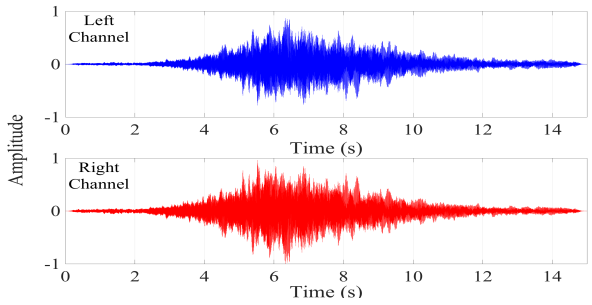

(b) Time plot of synthesised propeller plane.

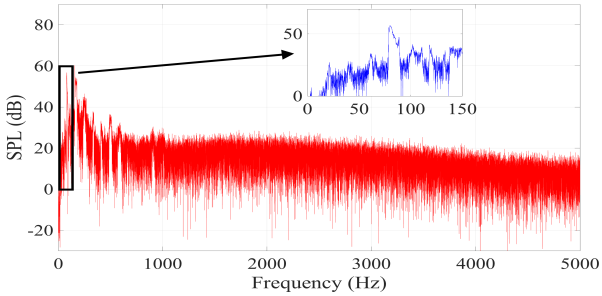

(c) Magnitude plot of recorded propeller plane.

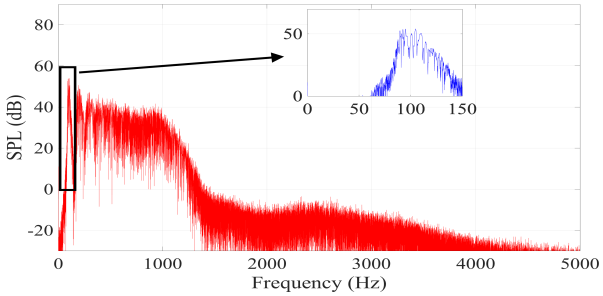

(d) Magnitude plot of synthesised propeller plane.

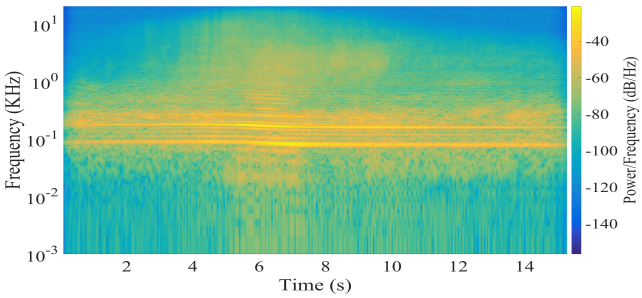

(e) Spectrogram of recorded propeller plane.

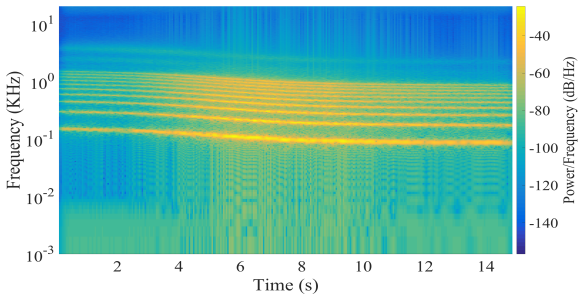

(f) Spectrogram of synthesised propeller plane.

Figure 5: Time plots and spectrograms of recorded and synthesised propeller powered aeroplane sounds.

in both figures as the amplitude peaks in the right channels marginally before peaks in the left channel. Another indicator is the average amplitude in the right channel plot of Fig. 5a being higher at the beginning of the clip, moving across to the left channel upper plot after the aircraft has passed.

This higher average amplitude level in the time plot of the recorded sound is not visible in the synthesised plot. The synthesised plot has no background environmental noise which is ever present in field recordings. However, it is believed that any background noise would be equally split between left and right channels in a field recording. This suggests the sound generating the higher average amplitude in the real recording is produced from the aircraft and therefore an aspect which is not captured by our model.

The rate of increase is different in both time plots. This could be due to different aircraft speeds or occlusion from structures masking the sounds in the real recording, making it difficult to draw any conclusions.

The magnitude spectra of both sounds are shown in Figs. 5c and 5d. The real recording has an initial peak which decreases rapidly until 500Hz and then much more gradually. In contrast the synthesised sound has an initial peak, then gradual decrease until about 1000Hz. After this there is a rapid drop in frequency content compared to the recorded noise. It is hypothesised that the wide band frequency content present in the real recording could from the engine, other components highlighted as sources in Fig. 2, and environmental noises. Our model is limited to 10 harmonics and

the additional frequency content in the real sounds may be a greater number of harmonics.

The value of the blade passing frequency in the synthesised model can be seen as a peak at ≈110Hz, relating to a three bladed propeller rotating at 2200 RPM. A similar peak is seen in the recorded magnitude spectrum occurring at ≈ 80Hz. If the recorded Cessna has three propellers they would be rotating at 1600 RPM or two blades rotating at 2400 RPM. Only 4 or 5 harmonic peaks are visible in Fig. 5c, with the second peak being the most prominent. In the synthesised sound the first peak is the highest and the remaining 9 decrease as calculated by the ten steps described in section 4.

The decrease in harmonic frequencies highlights the Doppler effect created as the aircraft passes the observer, visible in Figs. 5e and 5f. The frequency content of the recorded sound has the majority of the wide band noise when the aircraft is at its closest, ≈ 6 seconds. As this is not present throughout the clip it is a good indication that this is sound from the aircraft not captured by our model.

Subjective Evaluation

A double blind listening test was carried out to evaluate the effectiveness of our synthesis model. 20 participants, 6 female and 14 male, aged between 17 and 70, with a median age of 39, were asked to rate a number of sounds for authenticity. Each participant was presented with 4 test pages, in which each page contained 2 real samples, 2 samples from our model, 2 samples generated by sinusoidal modelling synthesis (SMS) [18] of a recording, and an anchor, which was created by downgrading the quality of our model. The anchors were created from the downgraded synthesis signal, to allow a thorough comparison of how plausible the synthesis method is compared to the recorded sample. It was expected that a low pass filtered sample, as used in the MUSHRA standard, would still be considered plausible, whereas a low quality downgraded anchor would encourage the full use of the scale and allow for better understanding as to effectiveness of the synthesis method.

The Web Audio Evaluation Tool [19] was used to build and run listening tests in the browser. It provides all the sample loudness normalisation, presentation order randomisation and results reporting in an intuitive way. This allowed test page order and samples on each page to be randomised. All samples were loudness normalised in accordance with [20].

The mean perceptual rating for all 24 clips is shown in Fig. 6. It can be seen that the real recordings received the highest mean plausibility rating and the anchor the lowest. There was little difference between the two synthesis methods. We performed one-way ANOVAs to determine the impact of synthesis method on the user authenticity ratings. Both synthesised methods were significantly worse than a recorded sample ($p < 0.0001$) but there was no significant difference between the synthesis methods ($p < 0.05$).

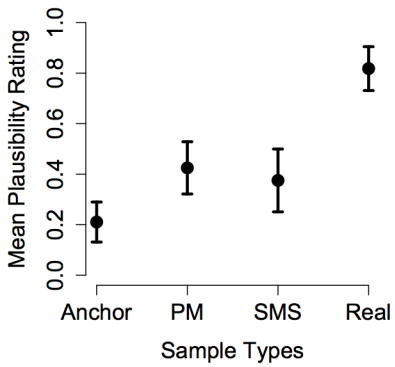

Figure 6: Mean plausibility rating for different sample types, including 95% confidence intervals. PM = Physical Model.

This was not unexpected and it is envisaged our model could be improved with further development and a better engine sound effect. The advantage of our synthesis method is the real-time operation with parameters based on actual aircraft behaviour and propeller characteristics. SMS techniques offer no method for deterministic parameter control. Common comments relating to our model were "decay too slow", "echo-like", "plausible", "warlike", "too smooth" and "I would expect more stutter".

6 DISCUSSION

A main challenge of designing the model was evaluating the relative levels of loading sound, vortex sounds and sound from the motor. No values were forthcoming from the literature, which is understandable considering the relationship will vary with motor type, blade design, and other design factors. Three gain sliders were provided in the model GUI to enable users to set these themselves, Fig. 7. The software is open source and users are able to modify the software to suit their requirements[14].

The motor powering the propellers may have a large influence on the perceived sound, especially when the observer is close to the plane. The engine model taken from [5] was designed to model a modern helicopter motor and hence may not capture inherent sounds associated with propellered aircraft. A more specific engine model would increase realism.

It is not ideal to compare our model with a recorded sound with limited details available. A more comprehensive objective and subjective evaluation of our propeller model would be comparing the sound produced by our model with a known aircraft, flying a known flight path past the observer. This would enable us to replicate the conditions exactly and

[14]A model demo and listening test sound files are available at https://code.soundsoftware.ac.uk/hg/propeller-model

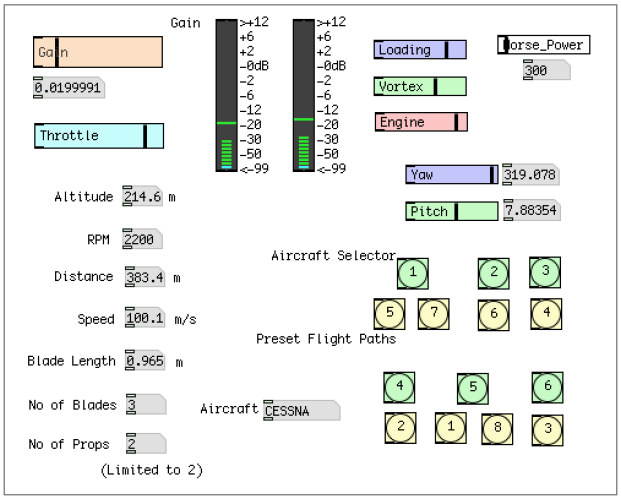

Figure 7: Pure Data GUI.

perform a direct comparison. It is also noted that an actual recording will include ground reflections and may include compression, reverb and other audio effects, enhancing the sound quality and adding to perceived realism; our model has no such processing.

By implementing more of the sound sources identified in Fig. 2 or increasing the number of harmonics synthesised, further improvements may be achieved, enhancing realism. Sounds from wheels, wheel wells, flaps and other components were not replicated and addition of these factors may increase authenticity. Our implementation requires approximating a number of plots in [12] to calculate the loading sounds. This may cause some details to be absent in our physical model.

The flight path and behaviour was programmed by the authors, an example is given in section 5. A future development could have parameters automated by attaching it to an aircraft object in a game engine, where the flight path is determined within gameplay[15].

7 CONCLUSION

Presented in this paper is a real-time physical sound effect synthesis model. It is based on semi-empirical equations identified from research in fluid dynamics and aerodynamics giving an approximation of the noise generated by a propeller. These equations and procedures were developed in order for design engineers to minimise the noise from the identified sources.

We have used these equations to produce a sound synthesis model that gives an acceptable approximation to actual sounds without the computational expense of solving the Navier - Stokes equations, common in computationally heavy CFD techniques.

Our interface provides a number of aircraft models. Although specific aircraft have been chosen as an example in our implementation, any propeller can be modelled given the correct dimensions and properties.

[15]An example of the sound effect added to a film clip is available at https://www.youtube.com/watch?v=xOclT8EiiU4

REFERENCES

[1] HH Heller, DG Holmes, and EE Covert. Flow-induced pressure oscillations in shallow cavities. *Journal of Sound and Vibration*, 18, 1971.

[2] H Fujita. The characteristics of the Aeolian tone radiated from two-dimensional cylinders. *Fluid dynamics research*, 42, 2010.

[3] PR Cook. *Real sound synthesis for interactive applications.* CRC Press, 2002.

[4] F Pfeifle and R Bader. Real-time finite-difference method physical modeling of musical instruments using field-programmable gate array hardware. *Journal of the Audio Engineering Society*, 63, 2016.

[5] A Farnell. *Designing sound.* MIT Press Cambridge, 2010.

[6] R Selfridge et al. Physically derived synthesis model of Aeolian tones. *Best Student Paper Award - 141st Audio Engineering Society Convention, LA, USA*, 29 Sept - 2 Oct 2016.

[7] R Selfridge, D Moffat, and JD Reiss. Real-time physical model for synthesis of sword sounds. *Sound and Music Computing, Espoo, Finland, 5 - 8 July*, (Accepted), 2017.

[8] R Selfridge et al. Real-time physical model of an Aeolian harp. *24th International Congress on Sound and Vibration, London*, 23-27 July 2017.

[9] K Janssens et al. Real-time synthesis and sound quality evaluation of interior aircraft noise. In *Proc. Forum Acusticum, Budapest, Hungary*, 29 Aug - 2 Sept 2005.

[10] D Berckmans et al. Model-based synthesis of aircraft noise to quantify human perception of sound quality and annoyance. *Journal of Sound and Vibration*, 311, 2008.

[11] LMBC Campos and FJP Lau. On a generalized multipole expansion with application to propeller design synthesis. *International Journal of Aeroacoustics*, 13, 2014.

[12] JE Marte and DW Kurtz. *A review of aerodynamic noise from propellers, rotors, and lift fans.* Jet Propulsion Laboratory, California Institute of Technology, 1970.

[13] ME Goldstein. Aeroacoustics. *McGraw-Hill International Book Co., 305 p.*, 1976.

[14] R E Donham and D J Osterholt. Utilizing test results to show adding flexibility of propeller blades is more representative than the classical rigid blade propeller whirl flutter analysis. In *Proceedings of International Forum on Aeroelasticity and Structural Dynamics (IFASD), Stockholm, Sweden*, 18-20 June 2007.

[15] EZ Stowell and AF Deming. Noise from two-blade propellers. *NACA Technical Report 526.*, 1936.

[16] D Brown and J B Ollerhead. Propeller noise at low tip speeds. Technical report, DTIC Document, 1971.

[17] PJW Block. Analysis of noise measured from a propeller in a wake. *NASA Technical Report*, 1984.

[18] X Amatriain et al. Spectral processing. *DAFX: Digital Audio Effects*, 2002.

[19] N Jillings et al. Web audio evaluation tool: A browser-based listening test environment. *Sound and Music Computing, Maynooth, Ireland*, 30 July - 1 August 2015.

[20] Recommendation ITU-R BS.1534-3. Method for the subjective assessment of intermediate quality level of audio systems. *International Telecommunication Union Radiocommunication Assembly*, 2015.